1H, 15N, and 13C backbone chemical shift assignments, secondary structure, and magnesium-binding characteristics of the Bacillus subtilis response regulator, Spo0F, determined by h...

ARTICLE *in* PROTEIN SCIENCE · SEPTEMBER 1995

Impact Factor: 2.85 · DOI: 10.1002/pro.5560040915 · Source: PubMed

Protein Science (1995), *4*:1801–1814. Cambridge University Press. Printed in the USA.

^{1}H, ^{15}N, and ^{13}C backbone chemical shift assignments, secondary structure, and magnesium-binding characteristics of the *Bacillus subtilis* response regulator, Spo0F, determined by heteronuclear high-resolution NMR

VICTORIA A. FEHER,[1] JAMES W. ZAPF,[2] JAMES A. HOCH,[2]
FREDERICK W. DAHLQUIST,[1] JOHN M. WHITELEY,[2]
AND JOHN CAVANAGH[3,4]

[1] The Institute of Molecular Biology and Department of Chemistry, University of Oregon, Eugene, Oregon 97403
[2] Department of Molecular and Experimental Medicine, The Scripps Research Institute, La Jolla, California 92037
[3] Department of Molecular Biology, The Scripps Research Institute, La Jolla, California 92037

(RECEIVED May 1, 1995; ACCEPTED June 13, 1995)

Abstract

Spo0F, sporulation stage 0 F protein, a 124-residue protein responsible, in part, for regulating the transition of *Bacillus subtilis* from a vegetative state to a dormant endospore, has been studied by high-resolution NMR. The ^{1}H, ^{15}N, and ^{13}C chemical shift assignments for the backbone residues have been determined from analyses of 3D spectra, ^{15}N TOCSY-HSQC, ^{15}N NOESY-HSQC, HNCA, and HN(CO)CA. Assignments for many side-chain proton resonances are also reported. The secondary structure, inferred from short- and medium-range NOEs, $^{3}J_{HN\alpha}$ coupling constants, and hydrogen exchange patterns, define a topology consistent with a doubly wound $(\alpha/\beta)_5$ fold. Interestingly, comparison of the secondary structure of Spo0F to the structure of the *Escherichia coli* response regulator, chemotaxis Y protein (CheY) (Volz K, Matsumura P, 1991, *J Biol Chem 266*:15511–15519; Bruix M et al., 1993, *Eur J Biochem 215*:573–585), show differences in the relative length of secondary structure elements that map onto a single face of the tertiary structure of CheY. This surface may define a region of binding specificity for response regulators. Magnesium titration of Spo0F, followed by amide chemical shift changes, gives an equilibrium dissociation constant of 20 ± 5 mM. Amide resonances most perturbed by magnesium binding are near the putative site of phosphorylation, Asp 54.

Keywords: bacterial signal transduction; CheY; phospho-relay; two-component signaling systems

Bacillus subtilis responds to nutrient deprivation and high cell density by expressing a group of gene products that result in a change of the cell morphology. These proteins transform the bacterium from a vegetative to a dormant form known as a dehydrated endospore. Commitment to grow or to begin this sporulation process is dependent on the action of a four-component phospho-relay system (Burbulys et al., 1991). The first two steps of this system involve induced autophosphorylation of either of

Reprint requests to: Frederick W. Dahlquist, The Institute of Molecular Biology and Department of Chemistry, University of Oregon, Eugene, Oregon 97403; e-mail: fwd@nmr.uoregon.edu; or John Cavanagh (at his present address), Wadsworth Center for Laboratories and Research, New York State Department of Health, Albany, New York 12201; e-mail: johnc@wadsworth.org.

Abbreviations: Spo0F, sporulation stage 0 F protein; Spo0B, sporulation stage 0 B protein; Spo0A, sporulation stage 0 A protein; KinA, kinase A protein; KinB, kinase B protein; CheY, chemotaxis Y protein; DQF-COSY, double quantum-filtered correlation spectroscopy; ROESY, rotating frame nuclear Overhauser enhancement spectroscopy; NOESY, nuclear Overhauser enhancement spectroscopy; HSQC, heteronuclear single quantum coherence; HMQC, heteronuclear multiple quantum coherence; HSMQC, heteronuclear single and multiple quantum coherence; HNCA, amide proton to nitrogen to α-carbon correlation; HN(CO)CA, amide proton to nitrogen to α-carbon of $i-1$ residue (via carbonyl) correlation; HNHB, amide proton to nitrogen to β-proton correlation; ^{1}H,^{15}N TOCSY-HSQC, total correlation spectroscopy combined with HSQC; ^{1}H,^{15}N NOESY-HSQC, nuclear Overhauser enhancement combined with HSQC; 2D, two-dimensional; 3D, three-dimensional; TPPI, time-proportional phase incrementation.

two kinases, KinA or KinB, and transfer of the phosphoryl group to the response regulator, Spo0F. A phosphotransferase, Spo0B, then catalyzes the transfer of the phosphoryl group from the Spo0F protein to the transcriptional activator/repressor, Spo0A. Spo0A~P plays a dual role; it represses expression of proteins that regulate the vegetative phase and activates gene expression important for sporulation (Hoch, 1993a).

Spo0F belongs to a large class of proteins, the response regulators, that participate in many different bacterial signal transduction pathways (Stock et al., 1989; Parkinson & Kofoid, 1992; Hoch, 1993a). Response regulators have diverse functions, for example, interaction with the flagellar motor and activation or repression of DNA transcription (Stock et al., 1989). Common to all these proteins is the presence of a regulatory domain of ~120 residues that becomes phosphorylated at a conserved aspartate residue in a magnesium-dependent reaction with a histidine autokinase. The formation of the acyl phosphate at the carboxylate of a conserved aspartate residue (Asp 54 in Spo0F) serves to activate the protein. Little is known of the physical manifestations of this activation. For some of the response regulators phosphorylation is thought to activate the protein through a conformational change. For example, mutations made in the chemotaxis response regulator, CheY, render the protein nonphosphorylatable, but these proteins can still generate the correct response in vivo (Bourret et al., 1993). Structural studies of phosphorylated CheY show conformational changes propagate away from the site of phosphorylation (Lowry et al., 1994). Spo0F, when phosphorylated, binds and transfers its phosphoryl group to Spo0B (Burbulys et al., 1991). This suggests that the signal transmitted from activated Spo0F is through transfer of the phosphate rather than exclusively through a conformational response.

Comparisons of primary amino acid sequences of response regulators to that of the chemotaxis protein, CheY, for which crystallographic and NMR structures have been determined, suggest that structural features are retained throughout this family of proteins (Volz & Matsumura, 1991; Stock et al., 1992; Bruix et al., 1993; Moy et al., 1994). Spo0F contains 54% sequence similarity with the *Escherichia coli* CheY protein. It contains the conserved active site residues D10, D11, D54, T82, and K104, in addition to many conserved hydrophobic residues that constitute the β-sheet core of the CheY protein. The sequence alignment suggests all these proteins have the doubly wound α/β global structure observed for CheY (Volz, 1993).

To date, 7 signaling pathways have been found in the bacterium *B. subtilis*, 18 in *E. coli*, and more than 100 examples of protein sequences that fit the conserved-residue criterion for response regulators in organisms ranging from bacteria, yeast, to higher eukaryotes have been reported (Msadek et al., 1993; Swanson & Simon, 1994). Evolution seems to have selected these structural and mechanistic qualities as a means to transmit signals within the cell. However, which structural and/or mechanistic features confer specificity to each protein to prevent crosstalk between different signaling pathways is still unresolved.

The backbone ^{1}H, ^{15}N, and ^{13}C resonance assignments, secondary structure, and global fold of apo Spo0F (124 residues, 14,286 Da) are reported here. These data reveal structural characteristics that are unique to Spo0F and general features analogous to the large response regulator family. In addition, an analysis of the magnesium ion binding to the protein is described. These studies constitute the initial steps necessary to provide the 3D structure of Spo0F in the apo-form and conformational responses to magnesium and phosphorylation.

Results

Resonance assignments

The general approach for assigning the backbone and side-chain resonances listed in Table 1 was based on the use of the ^{1}H,^{15}N HSQC spectrum as a fingerprint of the observable amides. Amide HN pairs identified in the HSQC were correlated to the backbone C^α through a 3D HNCA and to the side-chain protons via a 3D ^{1}H,^{15}N TOCSY-HSQC.

The ^{1}H,^{15}N HSQC has 111 of the expected 119 resonances correlating to backbone amides and 22 resonances representing the primary amines of asparagine and glutamine side chains (Fig. 1). Two additional amide peaks were later identified in spectra where either gradient or spin lock water saturation were used, namely Gly 14 and Met 55 (Met 2 is only observed for samples in potassium phosphate buffer). The 3D ^{1}H,^{15}N TOCSY-HSQC was analyzed by using strip plots (Driscoll et al., 1990) corresponding to each amide proton and its side-chain protons for a particular nitrogen chemical shift, yielding complete or partial side-chain proton assignments for 113 residues. TOCSY magnetization transfer was generally good except for leucines and the long spin systems, namely arginines and lysines. The 3D HNCA yielded backbone C^α resonance assignments for 112 residues. Using the H^N-N-C^α-H^α correlations and other side-chain protons derived from the TOCSY and HNCA spectra, many of the amides could be assigned to a particular spin system. Ten residues (six of seven glycines, three of four threonines, and one of two serines) were readily identifiable by their unique spin system pattern in the TOCSY spectrum.

Three ^{15}N specifically labeled Spo0F proteins, labeled with leucine, isoleucine, and lysine, were utilized to confirm the spin system assignments and to aid in sorting through several ambiguities observed in the 3D ^{1}H,^{15}N TOCSY-HSQC spectrum. These proteins were analyzed by ^{1}H,^{15}N HSMQC (label scrambling was not observed). The leucine-specific label identified several resonances, L18, L50, and L87, that were previously given alanine spin assignments based on incomplete side-chain cross-peak patterns in the 3D ^{1}H,^{15}N TOCSY-HSQC. The lysine-specific label was useful to distinguish lysine from arginine resonances in the TOCSY spectrum.

A 3D ^{1}H,^{15}N HNHB experiment was collected to distinguish the β protons from other side-chain protons observed in the 3D ^{1}H,^{15}N TOCSY-HSQC. The HNHB was collected with higher resolution in the F_1 dimension than the 3D ^{1}H,^{15}N TOCSY-HSQC, resulting in resolved resonances for several β-protons, which appeared degenerate in the TOCSY spectrum (data not shown).

Sequential assignment

Sequential assignments of Spo0F were accomplished in two phases. Initially, a 3D ^{1}H,^{15}N NOESY-HSQC was used together with the spin system data from the TOCSY to link regions with strong d_{NN} connectivities. These assignments were confirmed by the symmetry of the d_{NN}s, and the presence of $d_{\alpha N}(i, i+1)$, $d_{\alpha N}(i, i+3)$, and $d_{\beta N}(i, i+1)$ connectivities (Fig. 2). This resulted in sequential assignments primarily of α-helices, which

Table 1. *^{15}N, $^{13}C^{\alpha}$, and ^{1}H resonance assignments for recombinant Spo0F at pH 6.8 and 27 °C*

Residue	N	H^N	C^{α}	H^{α}	H^{β}	Others
Met 1						
Met 2	118.6	8.36	51.1	4.62	2.78	
Asn 3	128.9	8.35	51.4	4.96	3.01, 2.68	
Glu 4	118.4	8.31	56.0	4.37	2.14, 1.85	2.32
Lys 5	120.0	9.28	53.1	5.44	1.54	1.91, 1.70
Ile 6	121.8	8.86	57.0	4.87	1.23	0.98, 0.40, 0.28, −0.63
Leu 7	127.6	8.76	50.2	5.15		1.74, 1.00
Ile 8	128.7	9.05	59.4	4.37	1.82	1.62, 0.91
Val 9	128.3	9.08	58.4	4.92	2.37	0.64, 0.51
Asp10	123.2	7.96			2.32	
Asp 11						
Gln 12						
Tyr 13						
Gly 14	115.8	7.81	43.4			
Ile 15	120.2	6.96	59.9	3.89	2.03	1.35, 1.30, 0.87, 0.64
Arg 16	119.7	7.84	59.4		1.85, 1.66	
Ile 17	115.3	8.21	61.3	3.73	1.55	1.06, 1.04, 0.68, 0.63
Leu 18	123.8	7.25	55.7	4.14	1.73	
Leu 19	116.8	8.18	55.0	3.67	1.07	1.87
Asn 20	117.5	8.4	55.5	4.42	2.78, 2.55	
Glu 21	118.4	7.94	57.4	3.98	2.1	
Val 22	118.4	7.90	64.2	3.53	1.61	0.82, 0.32
Phe 23	116.7	8.12	58.4	4.55	2.91, 2.82	7.02, 6.94, 6.75
Asn 24	121.7	8.84	54.5	4.83	2.92, 2.69	
Lys 25	120.7	7.97	57.0	4.01	1.92	1.59, 1.41
Glu 26	115.6	7.30	54.0	4.14	2.36, 1.92	2.51, 2.14
Gly 27	103.9	7.53	42.0	4.19, 3.60		
Tyr 28	118.9	7.60	56.0	4.49	2.79, 2.31	7.08, 6.89
Gln 29	122.5	8.83	53.3	4.46	1.92	2.26, 2.05
Thr 30	115.4	8.02	57.9	5.41	4.05	1.05
Phe 31	120.0	8.86	54.0	4.78	3.16, 2.53	7.09
Gln 32	120.0	8.94	52.1	5.37	1.89	2.23
Ala 33	120.8	8.87	48.2	4.28	1.33	
Ala 34	120.5	8.43	48.2	4.19	1.41	
Asn 35	109.4	7.34	49.2	4.57	2.94	
Gly 36	107.4	9.15	45.3	3.71, 3.51		
Leu 37	122.4	7.99	56.0	4.01	1.51	1.70, 0.82
Gln 38	119.7	8.45	55.0	4.10	2.06	2.66, 2.37
Ala 39	119.5	7.82	53.1	3.69	1.28	
Leu 40	116.7	8.04	55.5	3.74	1.86, 1.36	
Asp 41	121.8	7.73	55.5	4.35	2.73	
Ile 42	119.5	7.84	63.2	3.55	1.79	1.69, 1.41, 1.10.81, 0.41
Val 43	121.2	8.55	65.7	3.23	2.00	0.82
Thr 44	113.8	7.92	65.2	3.64	4.28	1.14
Lys 45	118.7	7.80	57.0	4.01	1.70, 1.64	1.54, 1.37, 1.23
Glu 46	114.2	8.71	53.1	4.30	1.33	1.73, 1.37
Arg 47	112.8	7.61	52.6	4.23	1.77	1.41
Pro 48			60.6			
Asp 49	119.3	8.23	54.5	4.42	2.60	
Leu 50	117.8	7.63	51.6	5.03	1.25	
Val 51	125.5	8.83	57.9	4.96	1.86	0.77, 0.67
Leu 52	128.7	8.96	51.6	5.10	1.50	0.64
Leu 53	126.1	8.77	51.1	4.74	1.73	1.32, 0.82, 0.66
Asp 54	126.5	9.14		4.53	2.83, 2.64	
Met 55	120.4	9.55	53.1	4.37	1.96	2.41, 2.10
Lys 56	120.9	8.69	51.6	4.59	2.05	1.79, 1.51, 1.32
Ile 57	124.4	7.38	57.0	4.19	1.87	1.62, 1.06, 0.91, 0.69
Pro 58			59.9			
Gly 59	103.7	8.87	43.9	3.78, 3.55		
Met 60	122.2	7.69	53.1	4.28	1.87	2.39, 2.18
Asp 61	117.0	8.47	51.2	4.46	2.83	
Gly 62	111.4	8.87	45.8	4.05, 3.60		

(*continued*)

Table 1. *Continued*

Residue	N	H^N	C^α	H^α	H^β	Others
Ile 63	111.4	8.87	45.8	3.66	2.10	1.43, 1.35, 0.75, 0.61
Glu 64	121.0	7.41	56.9	3.92	2.05	2.23
Ile 65	118.8	8.11	62.3	3.55	2.05	1.52, 1.28, 0.80, 0.66
Leu 66	122.1	8.14	57.0	3.80	1.87	1.48, 0.73
Lys 67	117.5	8.26	58.4	3.73	1.77	2.55, 1.85, 1.59
Arg 68	118.2	8.22	57.0	3.90	1.81, 1.54	1.68
Met 69	120.6	8.84	58.9	3.71	2.23, 1.78	
Lys 70	116.4	7.53	54.5	4.05	1.80	1.55, 1.36
Val 71	117.7	7.16	62.3	3.64	2.05	1.04, 0.82
Ile 72	121.3	7.22	62.7	3.55		1.69, 0.91, 0.75
Asp 73	117.0	8.02	50.7	4.51	2.55, 2.23	
Glu 74	125.1	8.70	56.0	4.33	2.11, 2.02	2.25
Asn 75	116.4	8.33	50.6	4.74	2.87, 2.69	
Ile 76	123.6	7.42	60.3	3.87	1.81	
Arg 77	127.3	7.59	53.1	4.45	2.05, 1.41	1.66, 0.82
Val 78	122.7	8.69	58.4	4.87	1.60	0.64
Ile 79	127.9	9.11	58.7	4.14	1.46	1.40, 0.50, 0.37
Ile 80	120.4	7.66	57.0	5.15	1.92	1.69, 1.57, 0.91, 0.75
Met 81	121.4	8.72		5.78	1.89	2.37, 2.18
Thr 82	114.1	8.48	57.4	4.83	4.23	1.01
Ala 83	124.8	8.73	49.2		1.37	
Tyr 84	121.4	8.61	57.4	4.19	3.10, 2.90	7.09
Gly 85	111.9	8.47	42.4	3.51, 3.87		
Glu 86	121.5	7.85	53.6	4.37	2.07, 1.96	2.19
Leu 87	122.8	8.36	54.1	4.10	1.55	
Asp 88	119.5	8.45	54.5	4.28	2.62	
Met 89						
Ile 90	122.8	7.94	63.2	3.29	1.62	1.27, 0.41, 0.28
Gln 91	121.1	8.47	57.0	3.89	2.06, 1.97	2.32
Glu 92	120.5	8.81	57.4	3.92		2.22, 1.86
Ser 93	113.9	7.95	60.4	3.87	3.69, 3.55	
Lys 94	125.0	7.98	57.4	4.11	1.90	1.50, 1.28
Glu 95	121.6	8.04	57.0	4.01	2.09	2.37, 2.22
Leu 96	117.8	7.36	52.5	4.23	1.75, 1.50	
Gly 97	104.7	7.62	42.3	4.33, 3.65		
Ala 98	124.2	8.30	50.7	4.24	1.00	
Leu 99	122.8	8.90	55.5	3.87	0.91	1.09
Thr 100	105.9	7.18	57.0	4.28	4.42	0.76
His 101	120.2	8.14	51.8	5.71	2.64	6.45
Phe 102	119.7	8.65	broad	4.62	2.86, 2.46	6.97
Ala 103	125.2	8.52	47.8	4.92	1.19	
Lys 104	120.3	8.40	48.3	4.55	1.40	
Pro 105			59.6			
Phe 106	119.4	7.63	51.6	5.08	3.10	7.15, 6.89
Asp 107	122.9	9.22	50.6	4.83	2.87, 2.60	
Ile 108	126.7	8.77	60.8	3.69	1.87	1.37, 1.34, 0.82, 0.72
Asp 109	121.1	8.01	55.5	4.24	2.69, 2.55	
Glu 110	120.2	7.70	57.0	4.01	2.16	2.37
Ile 111	120.0	7.54	61.8	3.28	1.14	0.41, 0.23, 0.14, −0.39
Arg 112	121.6	8.22	57.9	3.83	1.96	1.64, 1.32
Asp 113	117.9	7.98	55.1	4.28	2.69, 2.52	
Ala 114	122.8	7.97	52.6	4.05	1.64	
Val 115	118.1	8.25	66.2	3.32	2.00	0.73, 0.23
Lys 116	116.7	7.81	57.4	4.46	1.78	3.02, 2.52
Lys 117	117.5	7.34	56.0	3.92	1.57, 1.36	1.19, 0.80
Tyr 118						
Leu 119	121.8	8.38	49.7	4.37	1.88, 1.08	1.60, 0.82
Pro 120			61.4			
Leu 121	123.8	8.26	52.6	4.28	1.50, 1.42	0.51
Lys 122	123.4	8.45	54.1	4.33	1.79	2.96, 1.34
Ser 123						
Asn 124	126.2	8.04	52.6	4.42	2.67	

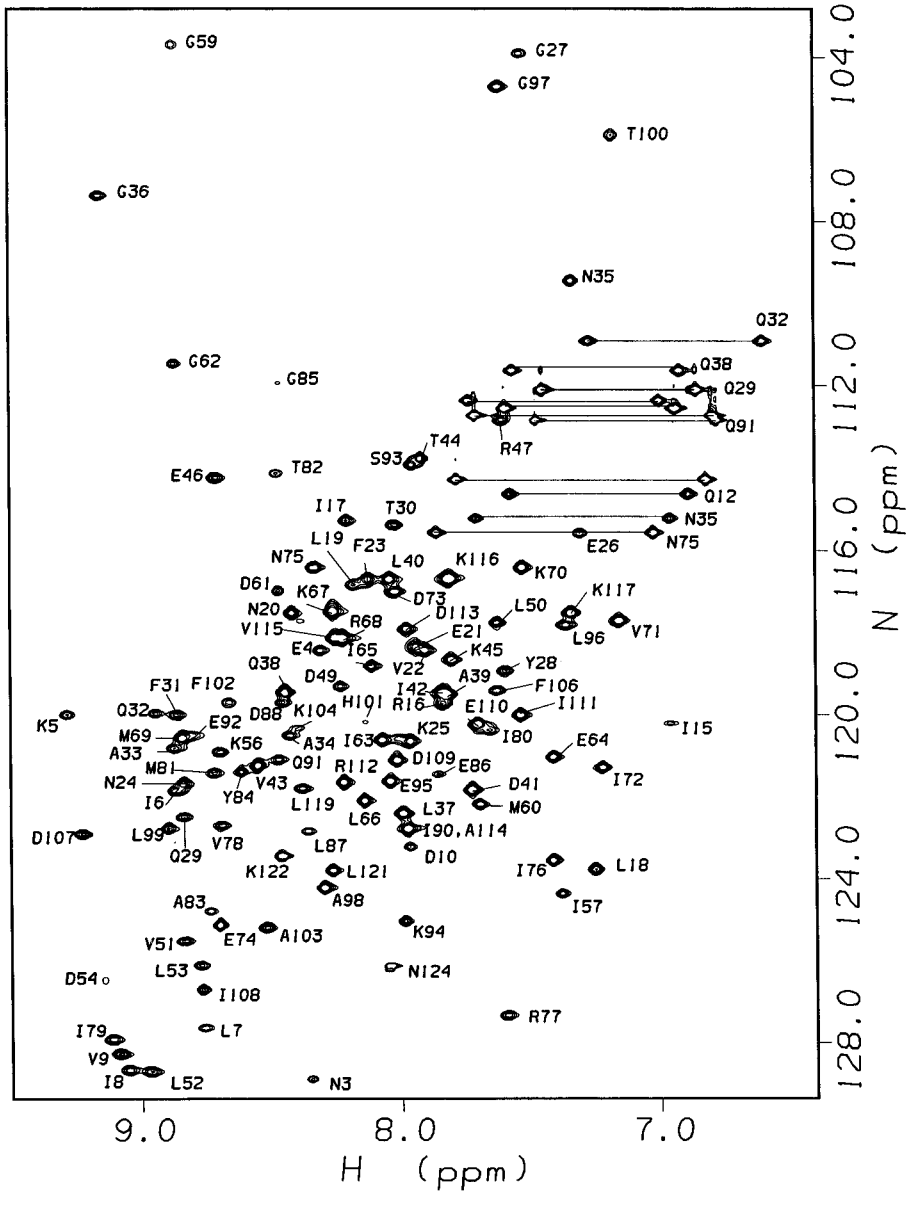

Fig. 1. $^{1}H,^{15}N$ HSQC spectrum of uniformly ^{15}N-enriched SpoOF in 25 mM Tris, 50 mM KCl, 0.02% NaN_3, 10% D_2O, pH 6.8, at 27 °C recorded on a Bruker AMX500 spectrometer. Nitrogen-correlated amide protons are labeled with amino acid type and sequence number.

constitutes 40% of the backbone. In the second phase, 3D $^{1}H,^{15}N$ NOESY-HSQC and 3D HN(CO)CA were used to work through regions of limited or ambiguous NOE information. Resonance overlap in the α-carbon region of the spectrum prevented the sole use of HN(i) correlation to the previous C^{α} derived from the HNCA/HN(CO)CA combination of spectra to link backbone resonances. Similarly, reliance on the NOESY was not possible for the β-strand regions because of possible ambiguities arising from strong $d_{\alpha N}(i, i+1)$ and $d_{\alpha N}(i, j)$. A combination of HN(i) to $C^{\alpha}(i-1)$ candidates from the HN(CO)CA and consistent intrastrand NOEs in the 3D $^{1}H,^{15}N$ NOESY-HSQC gave the remaining sequential backbone assignments. The specifically labeled protein samples confirmed that the correct sets of sequential connectivities were made. The HN(CO)CA also provided the α-carbon assignments for two proline residues.

Currently, 115 of the 124 backbone resonances have been assigned and are listed in Table 1. Residues not observed in spectra collected thus far are the first methionine (the N-terminal amine is usually not observed), aspartate 11 through tyrosine 13, methionine 89, tyrosine 118, serine 123, and two prolines. Included in Table 1 are many of the side-chain proton assignments and where possible β-protons have been indicated. In addition, proton resonances from aromatic rings are reported from analysis of 2D DQF-COSY and 2D NOESY experiments collected on a SpoOF sample dissolved in D_2O. Full ring assignments are not possible from these spectra alone because of significant resonance overlap (data not shown).

Secondary structure

Defining the secondary structure present in SpoOF was accomplished primarily from analysis of the 3D $^{1}H,^{15}N$ NOESY-HSQC. Three data sets were collected, two with mixing times of 100 ms and one with 140 ms. Differences in the number and

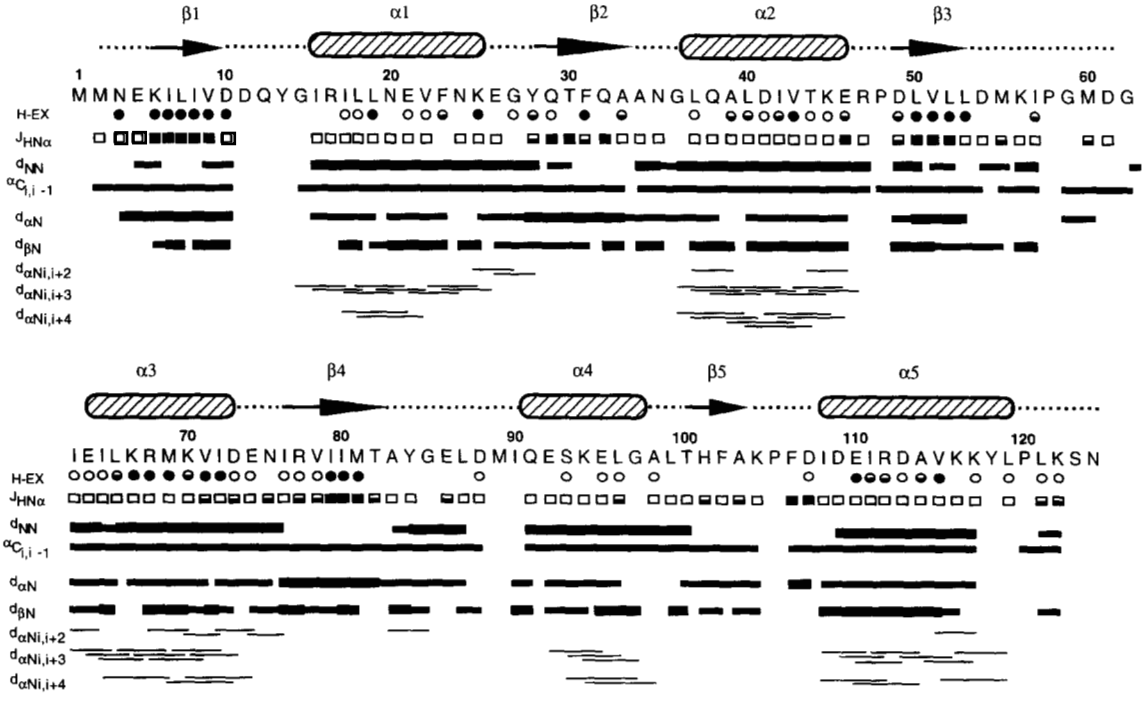

Fig. 2. Diagram of the NOE connectivities, hydrogen exchange rates, $^{3}J_{HN\alpha}$ coupling constants, and C^{α} (i, $i-1$) correlations (derived from HNCA/HN[CO]CA) for Spo0F. Sequential NOEs are divided into two classes, strong (thick bars) and weak to medium (thin bars). Hydrogen exchange rates (H-EX) are categorized into greater than 1×10^{-4} s^{-1} (closed circles), 1×10^{-3} to 1×10^{-4} s^{-1} (half-filled circles), and less than 1×10^{-3} s^{-1} (open circles). $^{3}J_{HN\alpha}$ coupling constants are divided into three groups, those greater than 8 Hz (filled boxes), 6–8 Hz (half-filled boxes), and less than 6 Hz (open boxes).

intensity of NOEs observed at the two mixing times are minor. $^{3}J_{NH\alpha}$ coupling constants measured by a $^{1}H,^{15}N$ HMQC-J, and amide hydrogen exchange rate constants were also used to define limits of secondary structure. A summary of these data is shown in Figure 2.

Helices

Strong $d_{NN}(i, i+1)$ and medium $d_{\alpha N}(i, i+3)$ connectivities outlined in Figure 2 are consistent with five α-helices spanning from G14 to K25, G36 to E46, I63 to D73, Q91 to G97, and I108 to L119. All these regions also contain many $d_{\alpha N}(i, i+4)$ NOEs, commonly observed in classical α-helices (Wüthrich, 1984, 1986). These helices are further supported by $^{3}J_{NH\alpha}$ coupling constants generally <6 Hz and amide hydrogen protection from deuterium exchange.

β-Strands

Strand limits are defined from strong $d_{\alpha N}(i, i+1)$ connectivities, slow deuterium exchange rate constants, and large $^{3}J_{NH\alpha}$ coupling constants (Fig. 3). Where there are discrepancies between $^{3}J_{NH\alpha}$, hydrogen exchange, and $d_{\alpha N}(i, i+1)$ connectivities in defining limits, $d_{\alpha N}(i, j)$ and $d_{NN}(i, j)$ were used. This criterion is consistent with β-strands extending from residues K5 to V9, Y28 to A33, L51 to D54, I76 to T82, and T100 to A103.

The across-strand connectivities, $d_{\alpha N}(i, j)$ and $d_{NN}(i, j)$, define the alignment of the strands with one another, requiring that they are parallel and order the strands in the sheet as β2-β1-β3-β4-β5 (Fig. 4). Consistent with this strand configuration, the most protected amides from hydrogen exchange, L50, V51, I79, and M81, are located in the central β-strands, 3 and 4. Strand 2 has alternating amide protection consistent with a strand at the solvent-exposed edge of the β-sheet. β-Strand 5 is relatively unprotected from deuterium exchange. All amide hydrogens of β-strand 5 exchanged by the first time point in the deuterium exchange experiment despite evidence implying the presence of extended chain, namely $d_{\alpha N}$ NOEs, $d_{\alpha N}(i, j)$ NOEs. The lack of deuterium exchange protection and the presence of medium-range $^{3}J_{HN\alpha}$ coupling constants indicate conformational flexibility in this region.

At the N-terminal end of β-strands β3 and β5, strong d_{NN} NOEs between D49 and L50 and L99 and T100 amides are consistent with the presence of β-bulges at these sites (Richardson et al., 1978). An across-strand $d_{\alpha N}$ between H^{α} of A98 and the amide proton of V78 also support the β-bulge observed at strand 5.

Multiple species

NMR samples used in our initial analysis gave HSQC spectra with 11 additional peaks to those observed in Figure 1. These additional resonances can be attributed to the presence of three Spo0F species (see Materials and methods). These correspond to (1) a species with the wild-type protein sequence and (2) two species lacking either one or both N-terminal methionines (see sequence in Fig. 2). The consequences of the three species can be seen in an $^{1}H,^{15}N$ HSQC of the ^{15}N-lysine specifically labeled protein (Fig. 5). K5, K116, and K122 have three peaks for

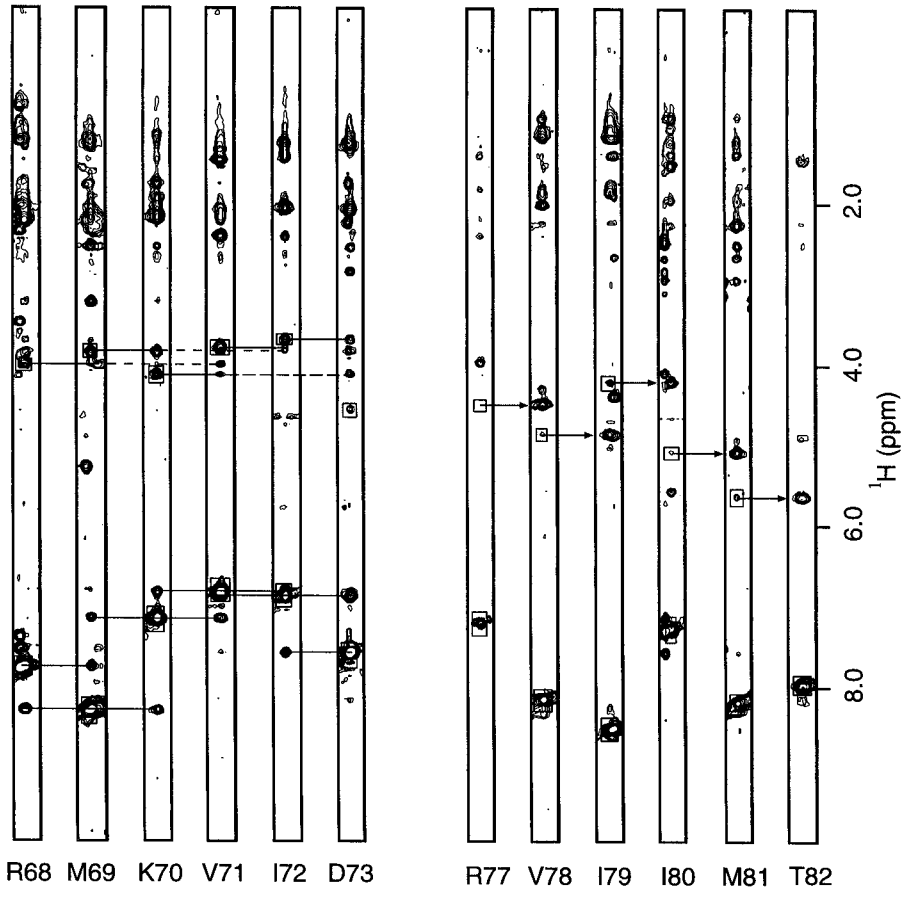

Fig. 3. Strip plots taken from 3D ^{1}H,^{15}N NOESY-HSQC at 100 ms collected on Bruker AMX600. The left set of strip plots illustrate d_{NN} and $d_{\alpha N}(i, i + 1)$ sequential NOEs (solid lines) confirming sequential assignments and $d_{\alpha N}(i, i + 3)$ connectivities confirming α-helical secondary structure. Strip plots on the right show arrows to indicate strong $d_{\alpha N}(i, i + 1)$ connectivities observed in this β-strand region. Peaks observed in the 3D ^{1}H^{15}N TOCSY-HSQC are indicated by boxes and represent diagonal protons or NOEs to intraresidue protons.

each amide proton assignment (peaks assigned to the minor species are boxed). The presence of the additional resonances in ^{1}H,^{15}N HSQC, 3D ^{1}H,^{15}N TOCSY-HSQC, and 3D ^{1}H,^{15}N NOESY-HSQC complicated sequential assignments in these regions until specifically labeled samples were made. A specifically labeled ^{15}N-leucine sample, produced with a very short incubation time following induction and judged greater than 95% full-length protein by mass spectrometry, gave an ^{1}H,^{15}N HSQC

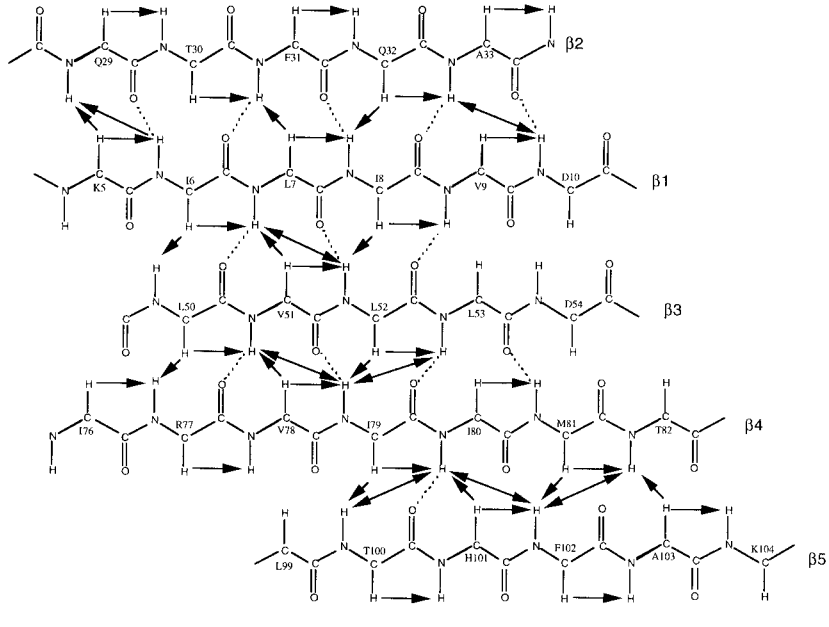

Fig. 4. Schematic diagram of a β-sheet for Spo0F. Sequential and across-strand H^{α} to H^{N} NOEs, indicated by arrows, define the orientation of this parallel β-sheet. Potential hydrogen bond partners, indicated by dashed lines, are deduced from amide proton protection in hydrogen exchange experiments.

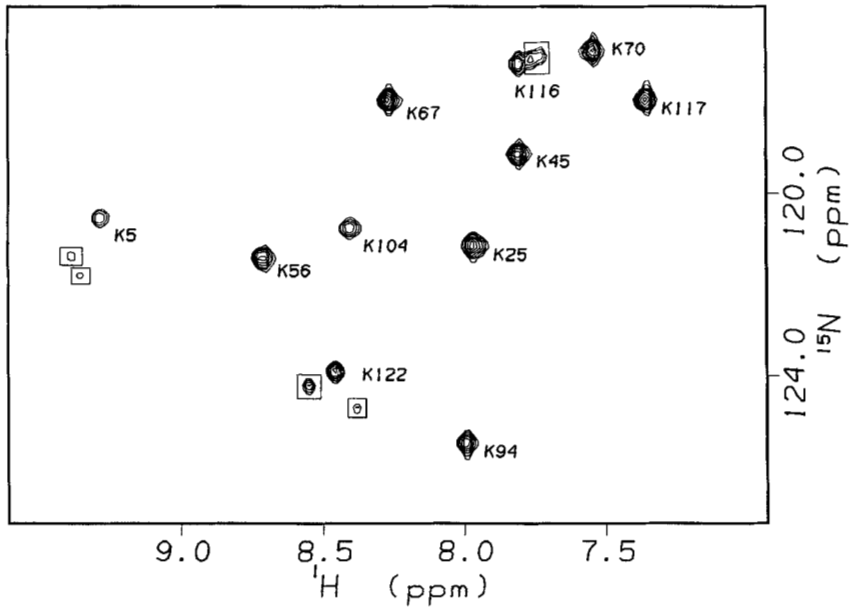

Fig. 5. ^{1}H,^{15}N HSMQC spectrum of Spo0F specifically labeled with ^{15}N-lysine. The Spo0F sequence contains 11 lysines. Additional resonances, outlined by boxes, represent lysines from Spo0F proteins that are modified at the N-terminus.

with only one resonance peak for each leucine, whereas previous samples had shown L119 and L121 to have three resonances to each. Following the completion of the backbone assignments, we find the regions that are sensitive to the multiple N-termini forms include the first β-strand (K5, I6), first few residues of β-strand 2 (Q29, T30), helix E (K116, L119), and the C-terminal end of protein (L121, K122).

Magnesium binding to Spo0F

Spo0F requires magnesium for phosphorylation by either KinA, KinB, or chemical phospho donors (Hoch, 1993b; Zapf et al., 1995). To characterize the affinity and structural consequences of magnesium binding, chemical shift changes of backbone amide proton resonances were followed by ^{1}H,^{15}N HSQC or ^{1}H, ^{15}N HSMQC spectra as magnesium concentration was increased. Tris was used as a buffer to avoid precipitation.

Amide resonances that had a total chemical shift change of greater than 50 Hz and were well resolved over the entire concentration range of 0–96 mM magnesium chloride were used to calculate the dissociation constant, K_d (Fig. 6). Six resonances, N20, G36, M60, T82, F102, and L119, met this criterion and gave K_d's of 20 ± 5 mM. Depletion of magnesium following the titration resulted in recovery of the initial apo form spectrum and demonstrated that any conformational changes observed were reversible.

Inspection of the chemical shift changes over increasing magnesium concentrations allow resonances to be classified into three groups: (1) those that do not change chemical shift; (2) a group whose chemical shift changes reflect a K_d for magnesium of 20 mM; and (3) a group whose chemical shift changes were not saturated at 96 mM magnesium chloride. The residues from group 2 exhibiting the largest chemical shift changes (greater than 80 Hz) are M55, K56, I57, and M60. These residues immediately follow the conserved site of phosphorylation, D54. Other resonances in group 2 that have shift changes greater than 50 Hz include N20, V22, T82, F102, and L119. The final group of resonances affected by increasing concentrations of magnesium chloride includes E86, L87, E92, and E110. The response of resonances in this region may reflect an unexpected, very low-affinity magnesium-binding site or an electrostatically coupled response to high ionic strength. In the case of the amide resonance for E110, a small response similar to that observed for group two resonances is followed by a much larger, nonsaturating chemical shift change.

Hydrogen exchange for magnesium-bound Spo0F

Changes in the rate constants for amide proton hydrogen exchange can indicate changes in solvent accessibility and relative strength of hydrogen bonds (Englander & Kallenbach, 1984). In order to determine if amide hydrogen protection patterns

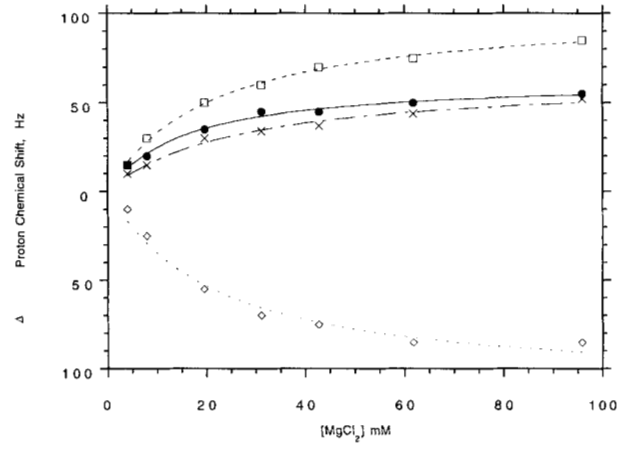

Fig. 6. Dependence of amide proton chemical shifts on magnesium chloride concentration. Curve fits for four amide proton resonances are shown. —●—, T82. --□--, M60. ---◇---, F102. --X--, L119.

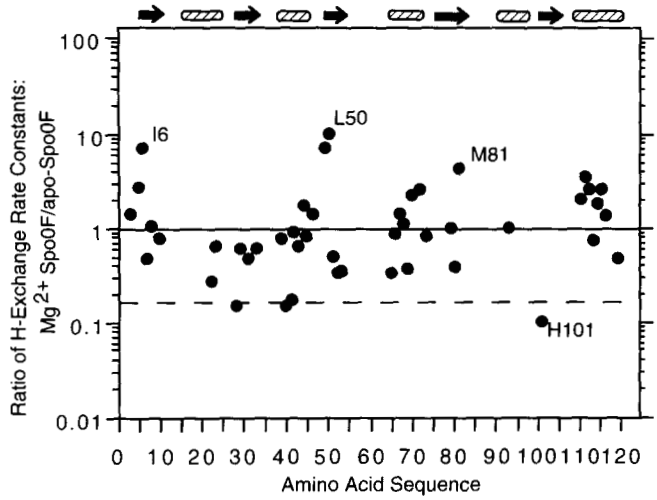

Fig. 7. Changes in hydrogen exchange between apo-Spo0F and magnesium-bound Spo0F represented as the ratio of the measured hydrogen exchange rates. Secondary structure elements are outlined, α-helices as dashed tubes, and β-strands as arrows. Dashed line indicates the theoretical maximum enhancement that can be observed for the protein containing ~15% magnesium-free protein.

changed as a consequence of magnesium binding, the deuterium exchange experiment was repeated on a sample containing 96 mM magnesium (the high-affinity site was 83% saturated). Figure 7 shows the log of the ratio of hydrogen exchange rate constants determined for the apo and magnesium-bound forms of Spo0F. Closed circles that are both greater than and less than 1 for many amide protons indicate regions of increased hydrogen exchange and enhanced protection from exchange, respectively, in the presence of magnesium chloride. A dashed line at 0.17 marks the theoretical limit of exchange inhibition due to the presence of ~17% apo-Spo0F at this magnesium chloride concentration. (The observed rate constant for the magnesium-bound sample = $0.83[k_{bound}] + 0.17[k_{free}]$ because the sample is not fully saturated. As the amide protection increases, the k_{bound} will approach zero and the maximal enhancement observed as a ratio of $k_{magnesium}$ sample over k_{free} reduces to 0.17.) This suggests when Spo0F is fully bound with magnesium ion the enhanced protection is greater than observed in this experiment. The enhanced protection for the amide hydrogen exchange rate constant of H101 is estimated to be near the theoretical limit. Its hydrogen exchange rate constant could not be determined directly in the apo-Spo0F because it exchanges prior to the first time point collected. A minimum value of 1×10^{-3} s^{-1} was assigned to determine the ratio and in the presence of 96 mM magnesium chloride the protection falls in the medium exchange rate constant range.

Discussion

The amide proton, amide nitrogen, α-proton, and α-carbon chemical shift assignments for 115 of 116 observable backbone resonances of Spo0F are reported (Table 1). The resonance that remains unassigned is very weak in HSQC spectra and α-proton or carbon resonances have not been observed by TOCSY or other coherence transfer experiments. Several residues remain undetected (Met 1, Asp 11 to Tyr 13, Met 89, Tyr 118, and Ser 123) and all are contained either at the extreme termini of the protein or in putative loop regions that may not be observed because the amide protons exchange with water. Instability of the sample at pH lower than 6.8 precludes slowing base-catalyzed amide hydrogen exchange. Many of the side-chain proton resonance assignments are also included, however, incomplete magnetization transfer or resonance degeneracy in the 3D ^{1}H,^{15}N TOCSY-HSQC do not allow complete assignment. In most cases, the α-protons were observed, with the exception of R16.

Sequential and medium range NOEs, assigned from analysis of a 3D ^{1}H,^{15}N NOESY-HSQC, shows that Spo0F is an $(\alpha/\beta)_5$ protein consisting of alternating α-helices and β-strands. Sequential assignments have been confirmed by HNC$^{\alpha}(i)$ to C$^{\alpha}(i-1)$ from the HNCA/HN(CO)CA experiments and the observed secondary structure has been deduced from NOE patterns (Fig. 2), deuterium exchange data, and $^3J_{NH\alpha}$ coupling constants. The core of the protein is defined by five β-strands arranged parallel to each other resulting in an overall strand order, β2-β1-β3-β4-β5. Current backbone NOE assignments are insufficient to correctly define the loops or turns that connect the helices and strands. These regions will be characterized when the tertiary structure is solved.

The secondary structure can be compared to the crystal and solution NMR structures of the homologous *E. coli* response regulator, CheY (Volz & Matsumura, 1991; Stock et al., 1992; Bruix et al., 1993; Moy et al., 1994). The alignment of the β-strands and α-helices are similar. Helices A, B, C, and β-strands 1, 2, 3, 4 are delineated at homologous residues by sequence alignment and the two β-bulges at the N-termini of strands 3 and 5 are observed in the same register (within ±1 residue for all NMR and crystal structures reported). Amide resonances of three residues in a loop near the active site are not detected (due to exchange broadening or solvent exchange saturation) in both Spo0F and CheY. These correspond to D11, Q12, and Y13 (Bruix et al., 1993; Moy et al., 1994). These results strongly suggest that the global fold for Spo0F is similar to that determined for CheY and confirms the analyses given by others based on primary sequence alignment that the overall fold for response regulators will generally be the same (Stock et al., 1992; Volz, 1993).

Despite the similar global fold, there are several subtle changes in the secondary structure that may constitute significant differences in local packing and the exposed protein surfaces (Fig. 8). Helices D and E have different lengths when the Spo0F primary sequence is aligned with CheY. Helix D begins four residues C-terminal down the sequence relative to helix D in CheY and helix E is three residues shorter than the corresponding helix E in CheY. Helix E in Spo0F has a proline at the C-terminal end, which likely acts as a helix terminator (Richardson & Richardson. 1988). In addition, β-strand 5 in Spo0F has NMR characteristics that are not consistent with a typical parallel β-strand. The sequential and across-strand NOEs are weaker than generally observed for β-strands (including those seen for other strands in Spo0F), the $^3J_{HN\alpha}$ coupling constants have intermediate values (6–7 Hz) and there is no protection of the backbone amide hydrogens from deuterium exchange. These observations suggest that β-strand 5 is not well ordered. Similar NMR parameters are not observed for β-strand 5 in CheY (Bruix et al., 1993; Moy et al., 1994). To summarize, helices D and E differ from

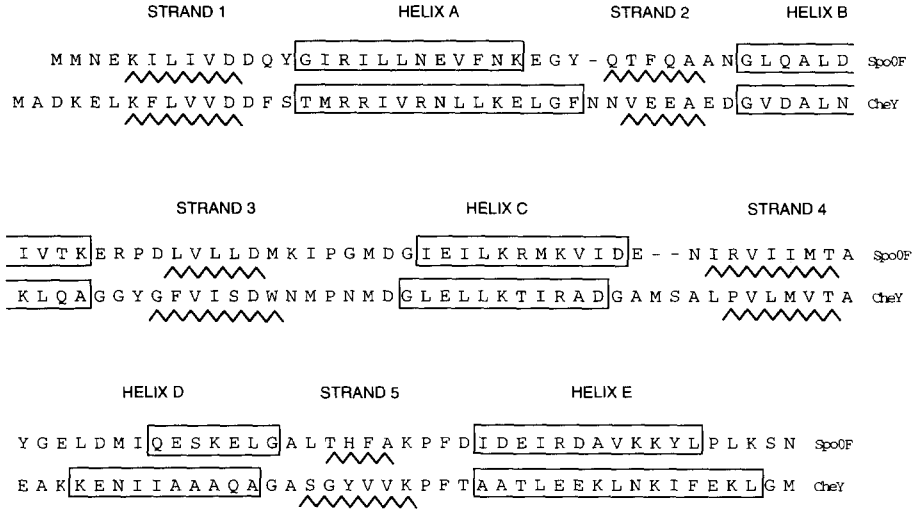

Fig. 8. Comparison of the secondary structure elements for SpoOF and *E. coli* CheY. The primary sequence alignment is taken from Table I of Volz (1993). The limits for the CheY secondary structure are the apo form NMR structure reported by Bruix and coworkers (1993).

those in the CheY structure by the absence of one helical turn and β-strand 5 is less well ordered in SpoOF. Interestingly, all of these differences map to a single face of the CheY protein.

The regions encompassing helices D and E, β-strand 5, and the loop between β-strand 4 and helix D in CheY are implicated in kinase binding (Swanson et al., 1995), are sensitive to phosphorylation (Lowry et al., 1994), and are important for interactions between CheY and the flagellar motor (Roman et al., 1992; Sockett et al., 1992). By analogy, differences between CheY and SpoOF observed in this region may define a protein surface that confers the different binding specificities these response regulators must have in their respective signaling pathways. In addition, the loops between β4 to helix D and β5 to helix E provide key placement of the side chains for conserved residues T87 and K109 in the vicinity of the acidic phosphorylation pocket in CheY. Changes in the relative placement of secondary structure defining these loops may lead to slightly altered geometric positioning and dynamics of these side chains in the active site pocket. However, this remains to be verified by elucidation of the high-resolution tertiary structure and biochemical and genetic analysis.

It is interesting to note that one crystal structure of the magnesium-bound form of CheY (Bellsolell et al., 1994) shows one turn of the N-terminus of helix D is unwound as compared to other crystal and solution structures (Stock et al., 1993; Moy et al., 1994) We find that the D helix of SpoOF is also unwound by one turn but this does not appear to be driven by magnesium binding. This may reflect an intrinsic structural dimorphism in this region of response regulator proteins. The potential functional role(s) of this feature is not yet clear.

Previously, SpoOF magnesium affinity was not determined because it lacks a convenient optical probe at the binding site. We report here a magnesium equilibrium dissociation constant of 20 ± 5 mM. This apparent low affinity for magnesium in vitro raises the question of the level of SpoOF magnesium saturation in vivo. Magnesium concentrations of greater than 100 mM will be required to saturate SpoOF if it has the same magnesium affinity in vivo. Soluble magnesium ion concentrations are estimated to be 1–2 mM in vivo (Alatossava et al., 1985). If the same low magnesium affinity is maintained in vivo, several mechanistic possibilities follow. Binding to the kinases, KinA or KinB, may alter the SpoOF magnesium affinity and ensure that the protein becomes phosphorylated only in response to the appropriate signal and by the correct kinase. Secondly, because magnesium is required for the autodephosphorylation in SpoOF (Zapf et al., 1995), the low affinity for magnesium may explain the long lifetimes observed for SpoOF~P in vitro. The observed $t_{1/2}$ for SpoOF in vitro is 12 h, three orders of magnitude longer than lifetimes observed for CheY (Lukat et al., 1990). Longer phosphorylated lifetimes may be important for the ability of SpoOF to interact with SpoOB, the target protein in this phosphorelay. Lastly, low magnesium affinity for SpoOF may play a role in regulating the population of SpoOF~P present in vivo. SpoOF~P transfers its phosphoryl group to SpoOB and ultimately to SpoOA, which then activates sporulation genes and represses factors that maintain vegetative life (Hoch, 1993a). Thus, controlling the population of SpoOF~P by regulation of its magnesium affinity and ultimately the levels of SpoOA~P present may provide another level of regulation for lifestyle change between the vegetative state and endospore formation.

Chemical shift responses to the binding of magnesium show that regions close to the active site residues of SpoOF are affected as well as those distant from this region. The largest chemical shift changes occur in the loop/turn following the probable site of phosphorylation, aspartate 54. In addition, some of the largest changes in amide hydrogen exchange rate constants between magnesium-bound and apo protein are observed in β-strands 1 and 3 (Fig. 7), strands that are linked to the active site by the presence of conserved residues D10, D11, and D54 at their C-terminal end. These observations strongly suggest that the magnesium-binding site in SpoOF is similar to the coordination site observed for CheY (Lukat et al., 1990; Stock et al., 1993; Bellsolell et al., 1994).

Smaller yet significant chemical shift changes are observed for regions removed from the putative binding site when magnesium binds. The N-terminal region of helix A shows perturbed chemical shifts upon magnesium binding. The chemical shift changes observed for residues T82, F102, and L119 can be interpreted from the alignment of the β-strands (Fig. 4). The hydrogen bonding network in the β-sheet connects T82 and F102 to the

putative site of magnesium binding, residues on β-strands 1 and 3. Large changes in the hydrogen exchange rate constants for amides M81 and H101 (Fig. 7) and chemical shift changes observed for residues T82 and F102 reflect structural changes that propagate from the active site through β-strands 4 and 5. These structural changes may also propagate to helix E. In the tertiary structure of CheY, helix E makes contacts to β-strand 5 (Volz & Matsumura, 1991; Bruix et al., 1993; Moy et al., 1994). In Spo0F, amide protons in this helix exhibit decreased hydrogen exchange protection (Fig. 7) and L119 has a large chemical shift in the presence of magnesium chloride. The significance of these changes is unknown because it is not known if Spo0F exists in the apo form in the unphosphorylated state, as suggested by its in vitro magnesium affinity, or whether its in vivo state is always in the magnesium-bound form.

We observed amide proton chemical shift changes at E86, L87, E92, and E110 in response to high concentrations of magnesium chloride. Analysis of these shifts shows that these chemical shift changes are far from saturated at 100 mM magnesium, suggesting either an unexpected second magnesium-binding site with much lower affinity than the one near the active site or that there is a localized electrostatic response to high ionic strength. The regions affected include the loop between β-strand 4 and helix D and the N-terminal end of helix E. The presence of a second binding site has not been previously reported for response regulators; however, in work done by Bellsolell et al. (1994) in which CheY was crystallized in the presence of 200 mM magnesium, large structural shifts in the loop region between β-strand 4 to helix D were observed. This response may be similar to that occurring in the same loop of Spo0F. A low-affinity binding site is unlikely to be populated at in vivo concentrations of magnesium, yet this phenomenon may reflect a region that becomes important in the phosphorylated form. Alternatively, this site may bind a different metal cation or provide an electrostatic surface that gives specificity for protein–protein interactions in vivo. Further studies are in progress to address these possibilities.

Concluding remarks

The studies presented here show that the *B. subtilis* response regulator Spo0F has a global fold consistent with a doubly wound $(\alpha/\beta)_5$ protein. There exist several subtle scaffolding differences when the secondary structure determined for Spo0F and another response regulator, CheY, are compared. These observations demonstrate the point that strong homologies in protein primary sequence can provide a basis for suggesting similarities in overall global fold, but the precise details of secondary structures, such as relative lengths of loops and helices, may differ. Protein active sites rely strongly on the precise geometry and dynamics of reactive side chains, indicating the subtle changes observed for Spo0F may play a large role. A 20-fold difference in magnesium affinity and a longer phosphorylation lifetime observed in Spo0F in vitro studies in comparison to values measured for CheY may be a reflection of this phenomenon. In addition, all observed differences in secondary structure and the flexible β-strand 5 map onto one face of the CheY tertiary structure. This region is implicated in kinase binding and flagellar motor interactions for CheY. This surface may define the way these proteins discriminate between cellular targets. The observed low affinity for binding of magnesium in vitro and the possibility of more than one metal binding site suggest new unexplored regulatory mechanisms in this phosphorelay system in vivo.

Materials and methods

Preparation of NMR samples

The overexpression and purification of recombinant Spo0F in *E. coli* has been accomplished using two protocols. Initially, the expression system and purification method (referred to as Protocol 1) was followed as described by Zapf and coworkers (1995). More recently, expression levels have been enhanced to give a yield of 15 mg of purified protein per liter of rich media using pET expression vectors (Novagen, Madison, Wisconsin). The spo0F open reading frame was PCR amplified from pKK0F (Zapf et al., 1995) using oligonucleotides complementary to the terminal portions of the spo0F gene and contained artificial *Nde* I and *Bam*H I sites. The spo0F gene was subcloned into the vector pET20b with *Nde* I and *Bam*H I. This construct was named pET0F. DNA sequence analysis confirmed that the pET0F contained wild-type Spo0F coding sequence. Uniform ^{15}N and ^{13}C labeling of Spo0F was accomplished by growing the pET0F containing *E. coli* BL21 DE3 strain culture in M9 minimal media with ^{15}N-labeled ammonium chloride and ^{13}C-labeled glucose (Isotec, Miamisburg, Ohio). Specifically labeled proteins with either ^{15}N-leucine, ^{15}N-isoleucine, or ^{15}N-lysine were prepared using the appropriate *E. coli* auxotroph and media conditions as described elsewhere (Muchmore et al., 1989). Spo0F was purified in a three-step procedure entailing DEAE-Trisacryl, Bio-Gel HTP hydroxylapatite, and gel-filtration column chromatography as described by Zapf et al. (1995). Addition of the hydroxylapatite column chromatography step served to remove a 30-kDa protein contaminant observed in Protocol 1. Spo0F obtained from the hydroxylapatite column was concentrated to no greater than 35 mg/mL and applied at a flow rate of 1 mL/min to a HiLoad 16/60 Sephacryl S-100 HR column equilibrated in 10 mM K_2HP0_4, 50 mM KCl, 0.02% NaN_3, pH 6.8. This method constitutes what is referred to as Protocol 2. Spo0F eluted as single peak and was judged pure by SDS-PAGE. N-terminal amino acid sequencing and mass spectrometry showed heterogeneity in samples purified from cell cultures that were incubated for periods greater than 8 h following induction. The heterogeneity arises from proteolysis of the N-terminal methionines resulting in samples containing 60–70% N-Met-Met-Asn-Glu-Lys–, 20–30% N-Met-Asn-Glu-Lys–, and 1–5% N-Asn-Glu-Lys–. Wild-type Spo0F has two N-terminal methionines (Trach et al., 1985; Fig. 2). Cell cultures prepared by Protocol 2 were typically harvested 5 h following induction to ensure samples had greater than 95% full-length protein, as judged by N-terminal amino acid sequencing. NMR samples were typically 1–2 mM Spo0F prepared in 10 mM potassium phosphate, 50 mM KCl, 0.02% NaN_3, 10% D_2O, pH 6.8, unless otherwise indicated. Samples are stable in these buffers at room temperature for at least 2 months before degradation is detected by SDS-PAGE or NMR spectroscopy.

NMR experiments

All spectra were collected on Bruker AMX500, AMX600, or General Electric GN Omega500 spectrometers at 27 °C. The experiments employed were ^1H,^{15}N HSQC (Bax et al., 1990; Norwood

et al., 1990); $^1H,^{15}N$ HSMQC (Zuiderweg, 1990); 3D $^1H,^{15}N$ TOCSY-HSQC (Marion et al., 1989a; Cavanagh et al., 1990); 3D $^1H,^{15}N$ NOESY-HSQC (Marion et al., 1989d; Zuiderweg & Fesik, 1989); HNCA (Ikura et al., 1990); HN(CO)CA (Bax & Ikura, 1991); $^1H,^{15}N$ HMQC-J (Forman-Kay et al., 1990); DQF-COSY (Piantini et al., 1982; Rance et al., 1983); 2D NOESY (Jeener et al., 1979); and HNHB (Archer et al., 1991). Unless otherwise indicated, all spectra were collected with a low power presaturation pulse for 0.8–1.1 s during the relaxation delay. TPPI-STATES procedure (Marion et al., 1989c) was employed for frequency discrimination in the indirect dimensions, except for the $^1H,^{15}N$ HSMQC and $^1H,^{15}N$ HMQC-J, where STATES procedure was used (States et al., 1982). Sampling delays were adjusted to equal one-half the dwell in the indirect dimensions of each experiment (F_1 for 2D, F_1 and F_2 for 3D experiments) so that a standard $-180°$ first-order phase correction could be applied when processing the data. This results in resonances folded in the F_1 dimension (2D) or F_2 dimension (3D) with the opposite phase of unfolded resonances (Bax et al., 1991). Data were processed using Felix software (Biosym Technologies) on either SGI Indigo or Sun Sparc II workstations. In general, spectra were first treated by convolution-based solvent reduction (Marion et al., 1989b) with function widths of 11–30, followed by cosine apodization, and zero-filled once. Spectral referencing for the proton dimension was based on a temperature calibration of the chemical shift for water (4.736 ppm at 300 K) as described by Hartel and coworkers (1982) and Dingermann and coworkers (1987). Reference frequencies for ^{15}N and ^{13}C nuclei detected in the indirect dimensions were calculated relative to values given for NH_3 and ethylene glycol as described by Live and coworkers (1984) and Bax and Subramanian (1986).

A 1.7 mM Spo0F sample prepared by Protocol 1 was used to collect the 3D $^1H^{15}N$ TOCSY-HSQC and first 3D $^1H,^{15}N$ NOESY-HSQC spectra on a Bruker AMX 500 spectrometer. The 3D $^1H,^{15}N$ TOCSY-HSQC was collected with $128 \times 48 \times 1{,}024$ complex points over spectral widths 5,800, 1,385.5, and 6,024 Hz for the F_1 (^1H), F_2 (^{15}N), and F_3 (^1H) dimensions, respectively, and 16 scans. Carrier frequencies were set at 4.74 ppm (F_3, F_1), 115.55 ppm (F_2). A 60-ms DIPSI-2rc sequence (Cavanagh & Rance, 1992) was employed to remove the ROESY peak contribution, enhancing TOCSY intensity. The 3D $^1H,^{15}N$ NOESY-HSQC was recorded with the identical number of scans, carrier frequencies, and spectral widths as for the TOCSY, except the number of points collected in the F_2 (^{15}N) dimension was changed to 32 complex points to reduce experiment time. A mixing time of 100 ms was used and a GARP sequence (Shaka et al., 1985) was employed to decouple nitrogen during the detection period. All experiments recorded subsequent to the TOCSY and NOESY just described were recorded using samples prepared by Protocol 2.

A 3D HNCA and an HN(CO)CA spectra were recorded on a Bruker AMX 500 spectrometer, with $27 \times 32 \times 1{,}024$ complex points over spectral widths of 1,383.5, 3,833.8, and 5,000 Hz for F_1 (^{15}N), F_2 (^{13}C), and F_3 (^1H), respectively, and 32 scans. The frequency in the F_3 dimension was set at 4.74 ppm for presaturation of water, then shifted to 7.96 ppm during the detection period. The carrier frequency for nitrogen was set to 115.55 ppm. The ^{13}C transmitter was optimized for selective excitation of the α-carbon region at 55.75 ppm and a null at carbonyl carbon frequencies. Carbonyl carbons were decoupled using a 180° carbon pulse of field strength 3.9 kHz, with an excitation null at the α-carbons during the carbon evolution period. A GARP sequence (Shaka et al., 1985) was used for decoupling nitrogen from amide protons during the acquisition period. Data processing differed from other spectra, the last points for the F_1 and F_2 dimensions were linear, predicted to 44 points, apodized with a squared-shifted sinebell, and zero-filled to 64 points in order to enhance resolution in the transformed spectrum.

Two additional 3D $^1H,^{15}N$ NOESY-HSQCs were recorded after correcting sample preparation conditions that lead to heterogeneity of Spo0F. One was recorded using a 1 mM Spo0F sample on a Bruker AMX 500 MHz and a mixing time of 140 ms. Spectral parameters for the F_1 (^1H) and F_3 (^1H) dimensions were similar to those described above for the 3D $^1H,^{15}N$ TOCSY-HSQC and NOESY-HSQC, $128 \times 1{,}024$ complex points and spectral widths of 6,024 Hz in F_1 and F_3, respectively. The number of complex points was increased from 32 to 38, the spectral width decreased to 1,114.8 Hz, and the carrier frequency shifted to 111.8 ppm to provide better resolution in crowded regions for the F_2 (^{15}N) dimension. A 2 mM Spo0F sample in 10 mM Tris, 50 mM KCl, 0.02% NaN_3, 10% D_2O, pH 6.8, was used for the second 3D $^1H,^{15}N$ NOESY-HSQC on a Bruker AMX600 spectrometer with a mixing time of 100 ms. This spectrum was recorded with $128 \times 32 \times 1{,}024$ complex points over spectral width of 6,250, 1,337.5, and 6,250 Hz in the F_1 (^1H), F_2 (^{15}N), and F_3 (^1H) dimensions. Carrier frequencies were set for 4.74 ppm (F_1, F_3) and 119.0 ppm (F_2).

Homonuclear 2D DQF-COSY and 2D NOESY were recorded on a Bruker AMX500 spectrometer with spectral parameters were set to $300 \times 2{,}048$ complex points over spectral widths of 6,002 and 6,250 Hz in the F_1 and F_2 dimensions and carrier frequency set to 4.74 ppm for both spectra. The DQF-COSY was collected with 64 scans per F_1 increment. The 2D NOESY spectrum was collected with a 120-ms mixing time.

The 3D HNHB experiment was recorded with a 2 mM Spo0F sample in 10 mM Tris, 50 mM KCl, 0.02% NaN_3, 10% D_2O, pH 6.8, buffer on a Bruker AMX600 spectrometer. It was recorded with $128 \times 32 \times 1{,}024$ complex points and spectral widths of 5,814, 1,666.7, and 5,814 Hz in the F_1 (^1H), F_2 (^{15}N), and F_3 (^1H) dimensions, respectively. Carrier frequencies were set to 4.74 ppm (F_1, F_3) and 116.11 ppm (F_2).

Hydrogen exchange

Deuterium exchange experiments were carried out by passing a 0.5-mL 1.5 mM sample prepared in 10 mM potassium phosphate, 50 mM KCl, 0.02% NaN_3, pH 6.8, through a G-25 Sephadex spin column (5 mL) equilibrated with the same buffer in 99.9% D_2O (Cambridge Isotopes Laboratories, Andover, Massachusetts). Ten $^1H,^{15}N$ HSMQC spectra (Zuiderweg, 1990) were collected over a 26-h period on a G.E. GN Omega 500 MHz spectrometer. The first spectrum was collected 9 min following application of the sample to the spin column. Spectral parameters were set to $128 \times 1{,}024$ complex points with spectral widths of 1,562.5 and 6,666.7 Hz in F_1 (^{15}N) and F_2 (^1H), respectively, and eight scans. Each spectrum required 33 min to collect. Amide peak volumes were measured using Felix Software (Biosym Technologies) and fitted (Kaleidagraph, Synergy Software) to an exponential curve, $V(t) = V_\infty + V_0 e^{-kt}$, where V_0 and V_∞ were initial and final peak volumes that were al-

lowed to vary to obtain the exchange rate constant, k. This process was repeated for another sample, 1.2 mM Spo0F, 25 mM Tris, 50 mM KCl, 96 mM $MgCl_2$, 0.02% NaN_3, 10% D_2O, pH 6.8. Identical spectral and processing conditions were used.

$^3J_{HN\alpha}$ coupling constants

A ^1H,^{15}N HMQC-J experiment was performed with spectral width 3,333 Hz and 1,024 complex points in F_1 (^{15}N) and F_2 (^1H) dimensions with 64 scans. Carrier frequencies were set to 117.5 ppm (^{15}N) and 4.74 ppm (^1H). The first point was linear predicted, followed by a gaussian apodization of 0.3, line broadening of −12 Hz, and zero-filling to 2,048 points in the acquisition dimension. The indirect dimension (F_1,^{15}N) was processed 5 times with different line-broadening values, −4, −6, −7, −8, −10 Hz, to estimate errors in measured $^3J_{HN\alpha}$ as outlined in Forman-Kay et al. (1990). The F_1 dimension for each matrix was apodized with a 0.9 gaussian window function zero-filled to 8,192 real points.

Magnesium titrations

Magnesium chloride titrations of Spo0F were initially attempted with samples in phosphate buffer. Precipitation made it difficult to achieve magnesium concentrations greater than 30 mM. Buffer conditions were changed to 25 mM Tris, 50 mM KCl, 0.02% NaN_3, 10% D_2O, pH 6.8. Tris does not significantly affect the NMR spectrum; chemical shifts were within 0.02 ppm for proton and 0.1 ppm for nitrogen. The only observable difference is that the resonance for Met 2 is not seen in spectra where Spo0F is in Tris buffer. The magnesium titration on a 1.2 mM Spo0F sample in Tris buffer conditions was accomplished by a series of ^1H,^{15}N HSMQCs recorded on a G.E. GN Omega 500 spectrometer with 128 × 1,024 complex points over spectal width of 1,562.5 in F_1 (^{15}N) and 6,666.7 Hz in F_2 (^1H) and eight scans. $MgCl_2$ stock solutions were prepared such that the total change in sample volume over the course of the titration was under 5%. For those resonances exhibiting fast exchange as a result of magnesium binding, plots of chemical shift changes, $\Delta\delta \pm 2$ (Hz), as a function of the total magnesium concentration, Mg_{total} (mM, ±18%), were fitted using the relationship,

$$\Delta\delta_{observed} = f_b \cdot \Delta\delta_{total}$$

where f_b is the fraction of magnesium-bound protein, and $\Delta\delta_{total}$ is the the total chemical shift change in (Hz). The fraction bound is related to the equilibrium dissociation constant, K_d (mM), and the magnesium ion concentration by the relationship,

$$f_b = [(Mg_{total})/(Mg_{total} + K_d)].$$

Values for K_d and $\Delta\delta_{total}$ were derived from iterative fitting to these equations. Initial apo form spectra were regenerated by treatment of the final titration point sample with two spin columns containing equal molar EDTA (to final magnesium chloride concentration). To confirm that initial samples were magnesium free, ^1H,^{15}N HSQC spectra were compared for the initial sample to a 1.3 mM sample treated with 30 mM EDTA. There were no detectable differences in the spectra.

Acknowledgments

We thank Mark Rance, Nick Skelton, Tsotne Djavakhishvili, David Lowry, and Susan Baxter for helpful discussions and technical assistance. We also thank Doug Barrick for comments on the manuscript. Support for this work comes from NIH grants GM19416 (J.A.H.), GM45727 (J.M.W.), GM33677 (F.W.D.), and The Stein Memorial Trust (T.S.R.I.). V.A.F. is supported by NIH Graduate Training in Molecular Biology and Biophysics grant GM07759.

References

Alatossava T, Jütte H, Kuhn A, Kellenberger E. 1985. Manipulation of intracellular magnesium content in polymyxin B nonapeptide-sensitized *Escherichia coli* by ionophore A23187. *J Bacteriol 162*:413-419.

Archer SJ, Ikura M, Torchia DA, Bax A. 1991. An alternative 3D NMR technique for correlating backbone ^{15}N with side chain Hβ resonances in larger proteins. *J Magn Reson 95*:636-641.

Bax A, Ikura M. 1991. An efficient 3D NMR technique for correlating the proton and ^{15}N backbone amide resonances with the α-carbon of the preceding residue in uniformly $^{15}N/^{13}C$ enriched proteins. *J Biomol NMR 1*:99-104.

Bax A, Ikura M, Kay LE, Torchia DA, Tschudin R. 1990. Comparison of different modes of two-dimensional reverse correlation NMR for the study of proteins. *J Magn Reson 86*:304-318.

Bax A, Ikura M, Kay LE, Zhu G. 1991. Removal of F_1 baseline distortion and optimization of folding in multidimensional NMR spectra. *J Magn Reson 91*:174-178.

Bax A, Subramanian S. 1986. Sensitivity-enhanced two-dimensional heteronuclear shift correlation NMR spectroscopy. *J Magn Reson 67*:565-569.

Bellsolell L, Prieto J, Serrano L, Coll M. 1994. Magnesium binding to the bacterial chemotaxis protein CheY results in large conformational changes involving its functional surface. *J Mol Biol 238*:489-495.

Bourret RB, Drake SK, Chervitz SA, Simon MI, Faulke JJ. 1993. Activation of the phosphosignaling protein CheY: II. Analysis of activated mutants by ^{19}F NMR and protein engineering. *J Biol Chem 268*:13089-13096.

Bruix M, Pascual J, Santoro J, Prieto J, Serrano L, Rico M. 1993. ^1H- and ^{15}N-NMR assignment and solution structure of the chemotactic *Escherichia coli* CheY protein. *Eur J Biochem 215*:573-585.

Burbulys D, Trach KA, Hoch JA. 1991. Initiation of sporulation in *B. subtilis* is controlled by a multicomponent phosphorelay. *Cell 64*:545-552.

Cavanagh J, Chazin WJ, Rance M. 1990. The time dependence of coherence transfer in homonuclear isotropic mixing experiments. *J Magn Reson 87*:110-131.

Cavanagh J, Rance M. 1992. Suppression of cross-relaxation effects in TOCSY spectra via a modified DIPSI-2 mixing sequence. *J Magn Reson 96*:670-678.

Dingermann T, Nerke K, Marschalek R. 1987. Influence of different 5′-flanking sequences of tRNA genes on their in vivo transcription efficiencies in *Saccharomyces cerevisiae*. *Eur J Biochem 170*:217-224.

Driscoll PC, Clore GM, Marion D, Wingfield PT, Gronenborn AM. 1990. Complete resonance assignment for the polypeptide backbone of interleukin 1β using three-dimensional heteronuclear NMR spectroscopy. *Biochemistry 29*:3542-3556.

Englander SW, Kallenbach NR. 1984. Hydrogen exchange and structural dynamics of proteins and nucleic acids. *Q Rev Biophys 16*:521-655.

Forman-Kay JD, Gronenborn AM, Kay LE, Wingfield PT, Clore GM. 1990. Studies on the solution conformation of human thioredoxin using heteronuclear ^{15}N-^1H nuclear magnetic resonance spectroscopy. *Biochemistry 29*:1566-1572.

Hartel AJ, Lankhorst PP, Altona C. 1982. Thermodynamics of stacking and of self-association of the dinucleoside monophosphate m^6/2A-U from proton NMR chemical shifts: Differential concentration temperature profile method. *Eur J Biochem 129*:343-357.

Hoch JA. 1993a. Regulation of the phosphorelay and the initiation of sporulation in *Bacillus subtilis*. *Annu Rev Microbiol 47*:441-465.

Hoch JA. 1993b. *Spo0* genes, the phosphorelay, and the initiation of sporulation. In: Sonenshein AL, Hoch JA, Losick R, eds. *Bacillus subtilis and other gram-positive bacteria*. Washington, DC: American Society for Microbiology. pp 747-755.

Ikura M, Kay LE, Bax A. 1990. A novel approach for sequential assignment

of ^{1}H, ^{13}C, and ^{15}N spectra of larger proteins: Heteronuclear triple-resonance three-dimensional NMR spectroscopy. Application to calmodulin. *Biochemistry 29*:4659–4667.

Jeener J, Meier BH, Bachmann P, Ernst RR. 1979. Investigation of exchange processes by two-dimensional NMR spectroscopy. *J Chem Phys 71*:4546–4553.

Live DH, Davis DG, Agosta WC, Coulburn D. 1984. Long range hydrogen bond mediated effects in peptides: ^{15}N NMR study of gramicidin S in water and organic solvents. *J Am Chem Soc 106*:1939–1941.

Lowry DF, Roth AF, Rupert PB, Dahlquist FW, Moy FJ, Domaille PJ, Matsumura P. 1994. Signal transduction in chemotaxis: A propagating conformation change upon phosphorylation of CheY. *J Biol Chem 269*: 26358–26362.

Lukat GS, Stock AM, Stock JB. 1990. Divalent metal ion binding to the CheY protein and its significance to phosphotransfer in bacterial chemotaxis. *Biochemistry 29*:5436–5442.

Marion D, Driscoll PC, Kay LE, Wingfield PT, Bax A, Gronenborn AM, Clore GM. 1989a. Overcoming the overlap problem in the assignment of ^{1}H NMR spectra of larger proteins by use of three-dimensional heteronuclear ^{1}H-^{15}N Hartmann–Hahn-multiple quantum coherence and nuclear Overhauser-multiple quantum coherence spectroscopy: Application to interleukin 1β. *Biochemistry 28*:6150–6156.

Marion D, Ikura M, Bax A. 1989b. Improved solvent suppression in one- and two-dimensional NMR spectra by convolution of time-domain data. *J Magn Reson 84*:425–430.

Marion D, Ikura M, Tschudin R, Bax A. 1989c. Rapid recording of 2D NMR spectra without phase cycling. Application to the study of hydrogen exchange in proteins. *J Magn Reson 85*:393–399.

Marion D, Kay LE, Sparks SW, Torchia DA, Bax A. 1989d. Three-dimensional heteronuclear NMR of ^{15}N-labeled proteins. *J Am Chem Soc 111*:1515–1517.

Moy FJ, Lowry DF, Matsumura P, Dahlquist FW, Krywko JE, Domaille PJ. 1994. Assignments, secondary structure, global fold, and dynamics of chemotaxis Y protein using three- and four-dimensional heteronuclear (^{13}C,^{15}N) NMR spectroscopy. *Biochemistry 33*:10731–10742.

Msadek T, Kunst F, Rapoport G. 1993. Two component regulatory systems. In: Sonenshein AL, Hoch JA, Losick R, eds. *Bacillus subtilis and other gram-positive bacteria*. Washington, DC: American Society for Microbiology. pp 729–745

Muchmore DC, McIntosh LP, Russell CB, Anderson DE, Dahlquist FW. 1989. Expression and nitrogen-15 labeling of proteins for proton and nitrogen-15 nuclear magnetic resonance. *Methods Enzymol 177*:44–73.

Norwood TJ, Boyd J, Heritage JE, Soffe N, Campbell ID. 1990. Comparison of techniques for ^{1}H-detected heteronuclear ^{1}H-^{15}N spectroscopy. *J Magn Reson 87*:488–501.

Parkinson JS, Kofoid EC. 1992. Communication modules in bacterial signaling proteins. *Annu Rev Genet 26*:71–112.

Piantini U, Sørensen OW, Ernst RR. 1982. Multiple quantum filters for elucidating NMR coupling networks. *J Am Chem Soc 104*:6800–6801.

Rance M, Sørensen OW, Bodenhausen G, Wagner G, Ernst RR, Wüthrich K. 1983. Improved spectral resolution in COSY ^{1}H NMR spectra of proteins via double quantum filtering. *Biochem Biophys Res Commun 117*:479–485.

Richardson JS, Getzoff ED, Richardson DC. 1978. The β bulge: A common small unit of nonrepetitive protein structure. *Proc Natl Acad Sci USA 75*:2574–2578.

Richardson JS, Richardson DC. 1988. Amino acid preferences for specific locations at the ends of α helices. *Science 240*:1648–1652.

Roman SJ, Meyers M, Volz K, Matsumura P. 1992. A chemotactic signaling surface on CheY defined by suppressers of flagellar switch mutations. *J Bacteriol 174*:6247–6255.

Shaka AJ, Barker PB, Freeman R. 1985. Computer-optimized decoupling scheme for wideband applications and low-level operation. *J Magn Reson 64*:547–552.

Sockett H, Yamaguchi S, Kihara M, Irikura VM, MacNab RM. 1992. Molecular analysis of the flagellar switch protein FliM of *Salmonella typhimurium*. *J Bacteriol 174*:793–806.

States DJ, Haberkorn RA, Ruben DJ. 1982. A two-dimensional nuclear Overhauser experiment with pure absorption phase in four quadrants. *J Magn Reson 48*:286–292.

Stock AM, Martinez-Hackert E, Rasmussen BF, West AH, Stock JB, Ringe D, Petsko GA. 1993. Structure of the Mg^{2+}-bound form of CheY and mechanism of phosphoryl transfer in bacterial chemotaxis. *Biochemistry 32*:13375–13380.

Stock AM, Mottonen JB, Stock JB, Schutt CE. 1989. Three-dimensional structure of CheY, the response regulator of bacterial chemotaxis. *Nature 337*:745–749.

Stock JB, Surette MG, McCleary WR, Stock AM. 1992. Signal transduction in bacterial chemotaxis. *J Biol Chem 267*:19753–19756.

Swanson RV, Lowry DF, Matsumura P, McEvoy MM, Simon MI, Dahlquist FW. 1995. Localized perturbations in CheY structure monitored by NMR identify a CheA binding interface. *Nature Struct Biol*. In press.

Swanson RV, Simon MI. 1994. Bringing the eukaryotes up to speed. *Curr Biol 4*:234–237.

Trach KA, Chapman JW, Piggot PJ, Hoch JA. 1985. Deduced product of the stage 0 sporulation gene *spo0F* shares homology with the Spo0A, OmpR, and SfrA proteins. *Proc Natl Acad Sci USA 82*:7260–7264.

Volz K. 1993. Structural conservation in the CheY superfamily. *Biochemistry 32*:11741–11753.

Volz K, Matsumura P. 1991. Crystal structure of *Escherichia coli* CheY refined at 1.7-Å resolution. *J Biol Chem 266*:15511–15519.

Wüthrich K. 1986. *NMR of proteins and nucleic acids*. New York: Wiley Interscience.

Wüthrich K, Billeter M, Braun W. 1984. Polypeptide secondary structure determination by nuclear magnetic resonance observation of short proton–proton distances. *J Mol Biol 180*:715–740.

Zapf JW, Hoch JA, Whiteley JM. 1995. A novel phosphotransferase activity of the *Bacillus subtilis* sporulation protein Spo0F that employs phosphoramidate substrates. *Biochemistry*. Submitted.

Zuiderweg ERB. 1990. A proton-detected heteronuclear chemical-shift correlation experiment with improved resolution and sensitivity. *J Magn Reson 86*:346–357.

Zuiderweg ERB, Fesik SW. 1989. Heteronuclear three-dimensional NMR spectroscopy of the inflammatory protein C5a. *Biochemistry 28*:2387–2391.